Continuous-flow multi-analyte biosensor cartridge with controllable linear response range†

Olivier Frey,* Sara Talaei, Peter D. van der Wal, Milena Koudelka-Hep and Nico F. de Rooij

Received 7th April 2010, Accepted 29th June 2010
DOI: 10.1039/c004851h

This article presents the design and fabrication of a microfluidic biosensor cartridge for the continuous and simultaneous measurement of biologically relevant analytes in a sample solution. The biosensor principle is based on the amperometric detection of hydrogen peroxide using enzyme-modified electrodes. The low-integrated and disposable cartridge is fabricated in PDMS and SU-8 by rapid prototyping. The device is designed in such a way that it addresses two major challenges of biosensors using microfluidics approaches. Firstly, the enzymatic membrane is deposited on top of the platinum electrodes *via* a microfluidic deposition channel from outside the cartridge. This decouples the membrane deposition from the cartridge fabrication and enables the user to decide when and with what mixture he wants to modify the electrode. Secondly, by using laminar sheath-flow of the sample and a buffer solution, a dynamic diffusion layer is created. The analyte has to diffuse through the buffer solution layer before it can reach the immobilized enzyme membrane on the electrode. Controlling of the thickness of the diffusion layer by variation of the flow-rate of the two layers enables the user to adjust the sensitivity and the linear region of the sensor. The point where the buffer and sample stream join proved critical in creating the laminar sheath-flow. Results of computational simulations considering fluid dynamics and diffusion are presented. The consistency of the device was investigated through detection of glucose and lactate and are in accordance with the CFD simulations. A sensitivity of 157 ± 28 nA/mM for the glucose sensor and 79 ± 12 nA/mM for the lactate sensor was obtained. The linear response range of these biosensors could be increased from initially 2 mM up to 15 mM with a limit of detection of 0.2 mM.

Introduction

It is undisputed, that the continuous and simultaneous monitoring of different, biologically relevant analytes is of great importance. Especially glucose and lactate are two key substances in both clinical and industrial applications: In medical health-care monitoring blood glucose levels and detecting hypo- and hyperglycemia,[1,2] in combination with lactate concentration as indicator for tissue oxygen levels,[3] in sports training analyzing the muscle metabolism in endurance activities[4] and in food manufacturing for fermentation processes[5] or quality control.[6] Further, if measurements are performed on site, small and inexpensive set-ups are required that are convenient in handling. These are mostly directly integrated in the production plant, analysis instruments or combined with sampling techniques as for example microdialysis probes.[7]

With the recent simplifications in microtechnological processes, the devices for the monitoring of these analytes trend from conventional flow-through cells mostly consisting of an assembled stack of multiple layers[7–9] towards microfluidic chips with integrated biosensors.[10–13] In many cases, the biosensor principle is based on the amperometric detection of hydrogen peroxide produced by the enzymes glucose oxidase (GOx) and lactate oxidase (LOx), respectively, immobilized on dedicated microelectrodes.

Combining microfluidic techniques and electrochemical detection methods provide the advantage of precise manipulation of low sample-volumes in miniaturized channels, high sensitivities and fast response times.[14,15] However, when designing microfluidic devices it is important to consider their allover life cycle (from fabrication to disposal) and to optimize their use for all involved parties (manufacturer, distributor, end-user). Only in this way the benefits of such systems can be maximally exploited. In general, they are designed as a flow-through channel, where biosensors are directly integrated in. When several substances have to be detected simultaneously, chemical cross-talk between adjacent microelectrodes can become problematic,[16,17] especially when the biosensors' principles are based on similar biochemical reactions such as in the present case. This effect can be reduced or eliminated by placing the electrode in a dedicated containment,[10,18] applying a cross-talk-reducing membrane above the biosensors,[12,16,19] introducing a separator between the electrodes[20] or by using the laminar-flow conditions at low Reynolds numbers. In the latter approach, the microelectrodes are arranged in a column perpendicular to the direction of the flow.[11]

The realization of these devices implicates two further important challenges. First, the microelectrodes in the

École Polytechnique Fédérale de Lausanne (EPFL), Institute of Microengineering (IMT), Sensors, Actuators and Microsystems Laboratory (SAMLAB), Rue Jaquet-Droz 1, 2000 Neuchâtel, Switzerland. E-mail: olivier.frey@epfl.ch; sara.talaei@epfl.ch; peter.vanderwal@epfl.ch; mkoudelka@eblcom.ch; nico.derooij@epfl.ch; Fax: +41 32 720 5711; Tel: +41 32 720 5574

† Published as part of a themed issue dedicated to Swiss Research: Guest Editor Professor Viola Vogel.

flow-through channel have to be functionalized with an enzyme membrane to create selective sensors. Normally, this is performed as an intermediate step, splitting the fabrication process in two parts before the flow-through channel is sealed by its cover. This is inconvenient, because (a) the device cannot be fully processed in a single run, (b) subsequent fabrication processes are restricted because they can harm the temperature-sensitive enzymes and (c) device shelf lifetime is limited by the enzyme stability. Further, the local and reliable deposition of the enzymatic layers on microelectrodes mostly requires high-priced, low-volume dispensing equipment,[12] photolithographic[21,22] or electrochemical[23,24] processes. The second challenge lies in the low linear response range of both biosensors, which in many cases does not match the requirements of their application. Therefore, different additional membranes have been proposed to be deposited on the top of the enzymatic membranes acting as diffusion-limiting layer for the analyte.[9,10,12,22,25,26] However, the deposition of these layers adds an additional functionalization step and has to ensure, that in the same time, they are not limiting essential co-substrates of the enzyme reactions (*e.g.* oxygen).

In this contribution, we present a microfluidic device for the detection of glucose and lactate fabricated by a straightforward rapid prototyping process using a combined SU-8/PDMS approach. It is operated as a disposable cartridge by an external desktop unit controlling fluid-flow and data acquisition. Electrode functionalization is performed after completed cartridge fabrication by the use of an on-chip focused dispensing approach. This allows to locally and reproducibly cover the microelectrode with the specific enzymatic membrane from outside the cartridge using simple dispensing. The linear response range of the biosensor can be adjusted on-line during the measurement. This is achieved by a stream of buffer solution introduced beneath the sample stream, generating a dynamic diffusion layer. Its thickness can be adjusted by the control of the buffer flow-rate thus adapting the sensitivity and linear region.

Concept and layout of the microfluidic device

The layout of the microfluidic system with dimensions 6.3 cm × 2.2 cm is presented in Fig. 1A. The sample is introduced in a straight microchannel with a cross-section of 370 μm × 800 μm (height × width) and a total length of 45.8 mm. At the end of the channel, three Pt-microelectrodes (80 μm × 3000 μm) are placed in parallel to each other for the detection of three different analytes at the same time. A fourth, larger, elliptic electrode located further downstream is used as combined pseudo-reference/counter electrode (1.3 mm^2). All microelectrodes are addressed by larger electrode pads on the side of the system. The

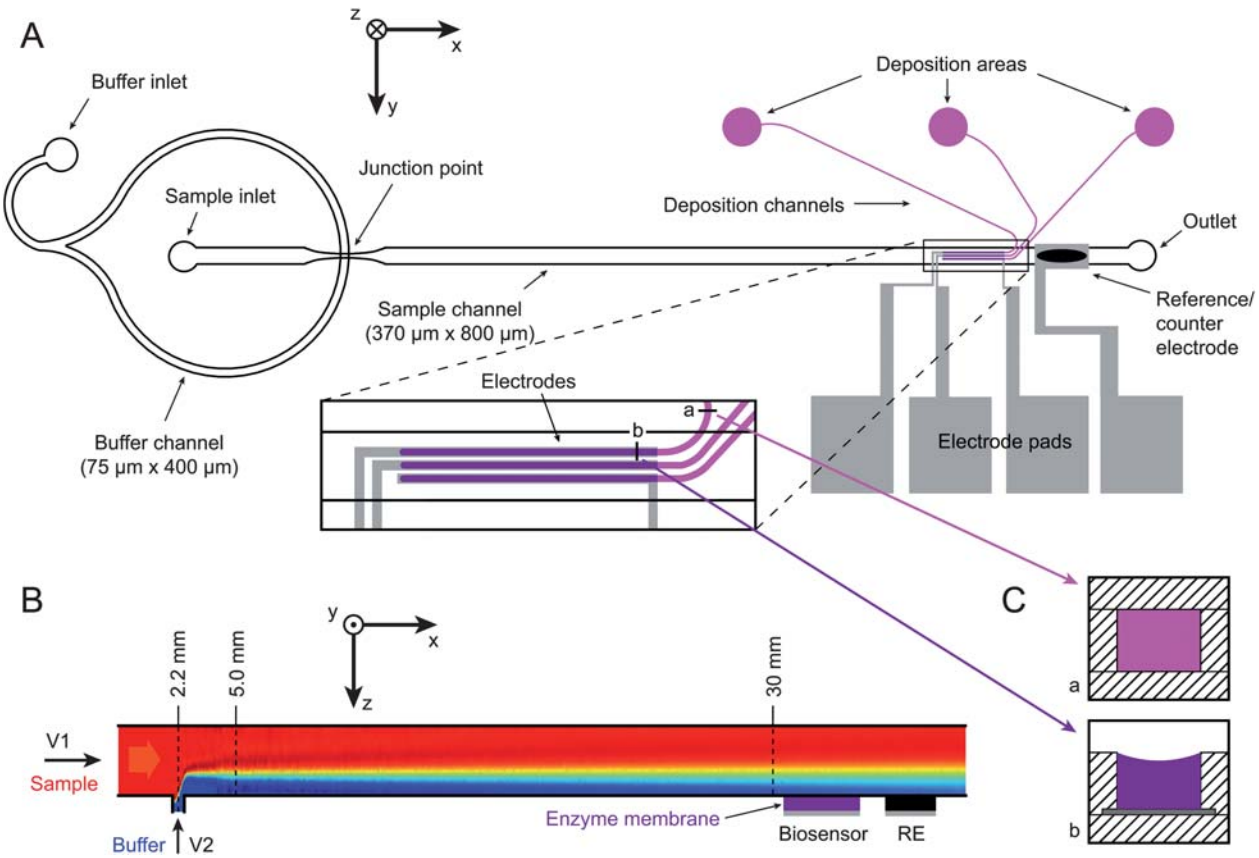

Fig. 1 (A) Top view of the microfluidic layout. The sample is directed through a straight channel comprising three parallel-aligned biosensor electrodes and a combined Pt pseudo-reference/counter electrode at the end. The microelectrodes are addressed by pads at the lower part and coated with an enzymatic layer using the integrated capillary-driven deposition channels (see text for details). The buffer solution is introduced at the junction point by a second channel from beneath creating sheath-flow. (B) schematically illustrates the cross-section along the length axes of the flow channel. The analyte diffuses from the sample solution through the buffer when travelling along the channel. (C) Cross-sections of the deposition channel in the covered region (a) and at the uncovered electrode site in the flow-through-channel (b).

parallel positioning along with the laminar flow present in the microchannel prevents cross-talk.

The functionalization of the microelectrodes consists of a coating with an enzymatic membrane. We have chosen to decouple this from the fabrication of the cartridge. Advantages are that shelf life of the cartridge is not limited and it can be decided later by either the manufacturer, a third party or the end user with which membranes to functionalize the electrodes. This is realized by integrating a capillary-driven deposition channel for each microelectrode on the cartridge. The freshly prepared enzyme solution is dispensed in the deposition area outside the flow-through channel and fills the complete deposition channel by capillary force.[27,28] In this way the solution is automatically guided through the covered region (Fig. 1Ca) before reaching the flow-through channel, where the deposition channel is not covered any more and forms the active electrode site (1Cb). The larger cross-section of the main channel creates a capillary pressure barrier, which prevents an overflow. The solution cross-links within a few minutes and immobilizes the enzyme. Each channel forms a containment that mechanically stabilizes the specific membrane and additionally helps to reduce chemical cross-talk between different electrodes. Thickness and spatial resolution of the deposition is automatically controlled by the design of the deposition channel and is independent of the applied volume of the liquid droplet (0.5–2 μl), that thus has not to be precisely controlled (= on-chip focusing). With this method, all three electrodes can be independently coated by different functional layers creating specific biosensors laterally separated by 75 μm.

A drawback of glucose and lactate biosensors is the too low linear response range because the reaction can become limited in oxygen at high concentrations. A possible solution is a diffusion-limiting layer applied over the enzyme membrane that restricts the analyte from reaching the electrode while not influencing O_2-diffusion. This increases the linear response range, though at a lower resulting sensitivity of the system. The deposition of such a perm-selective membrane can additionally be controlled by altering its thickness[26] or cross-linking parameters[10] to adjust the response characteristics for a specific application. In this contribution, we use a liquid diffusion layer together with the laminar-flow conditions in the microchannel. A flow of buffer solution is introduced below the sample-flow creating sheath-flow in the flow-through channel.

Its thickness can be dynamically controlled by the flow-rate of the buffer solution (see Fig. 1B) and thus the linear response range and sensitivity adjusted on-line. Using this approach, essential reaction co-substrates as for example oxygen are continuously replenished.

Of critical importance in this approach is the generation of a homogeneous thickness of the fluid layers across the microchannel. Sheath-flow in a horizontal arrangement in microfluidic devices has been multiply presented – hydrodynamic focusing is the most popular example.[29] It has been employed especially for the investigation of reaction kinetics[30–32] using its fast diffusion-controlled mixing characteristics. For a vertical arrangement, while keeping fluidic connections on one side and fabrication as simple as possible, this issue becomes more challenging. Very recently, Simonnet *et al.*[33–35] and Zhuang *et al.*[36] presented similar solutions of three-dimensional focusing systems for cell cytometry and reaction kinetics applications. Kaufmann *et al.*[37] implemented a three-layer flow-system using silicon micromachining, whereas Hofmann *et al.*[38,39] fabricated a 3D-microchip out of PDMS. The latter used the planar sheet geometry to confine a sample flow to a sensor surface and enhance sample delivery, however this is the opposite of our application. In our microfluidic system, we had to geometrically optimize the junction point, where the buffer solution meets the flow-through channel from below, to generate two planar sheets of liquid above each other.

Due to the planar fabrication process, the buffer solution has to be provided sideways beneath the sample flow.[33,36] Our flow-through channel is rather wide with a low aspect ratio (370 μm × 800 μm) that is required since multiple electrodes are placed perpendicular to the channel further downstream. Introducing the buffer from the side will result in a curved liquid plane between the two solutions. Therefore the flow-through channel was locally narrowed down to 200 μm thus substantially changing the aspect ratio and strongly reducing this effect.[35] A re-widening of the channel results in a lateral scaling and due to laminar flow condition, an improved homogeneity of the two-layer flow is achieved.

Results and discussion

Electrode functionalization

Electrodes could be reproducibly coated using different, optimized enzyme solutions. Complete filling of the deposition channel occurred in less than 2 s stating good wetting-characteristics of the surfactant-enriched enzyme solution. Due to the capillary pressure barrier between the deposition channel and main channel, no overflow into the sample channel or adjacent deposition channels could be observed (a) optically during deposition and (b) analytically when measuring simultaneously from all three electrodes. Complete cross-linking occurred after 2-3 min without significant shrinkage. Fig. 7B shows a photograph of a colored, cross-linked enzyme membrane on one of the electrodes. A similar deposition method was used in a previous publication for silicon microprobes.[40]

Homogeneous sheath-flow

A constant thickness of the diffusion layer over the whole channel width is required to ensure a proper functioning of the adjustment of the linear response range on all three, parallel-aligned biosensor electrodes. Different designs of the junction point have first been tested experimentally (not shown). Here we focus on the most suitable that has been further assessed experimentally and using CFD simulations that were compared with the basic, straight-channel design.

CFD simulations. Fig. 2 illustrates computed results of the flow and diffusion behavior using two different junction point designs and varying flow-rates of buffer and sample solution. It compares the laminar flow of the two liquids with (A) an unchanged cross-section (370 μm × 800 μm) of the straight flow-through channel over its whole length and (B) a narrowing down to a width of 200 μm (at same height: 370 μm) at the junction point (*cf.* Fig. 1). For the sample here we have chosen

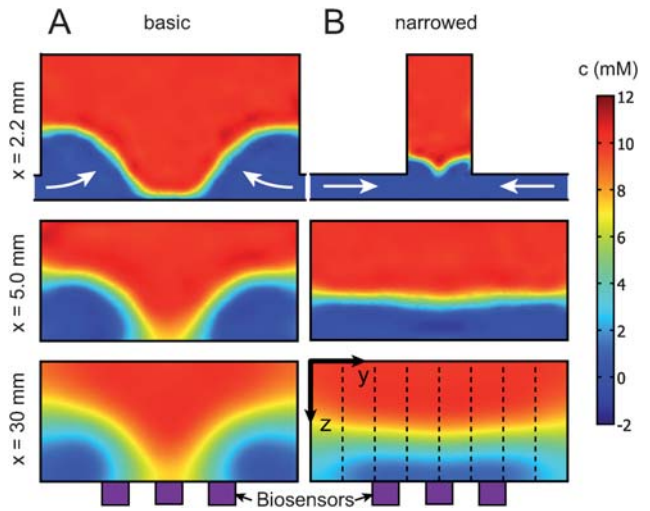

Fig. 2 Computed simulations of the cross-sectional concentration distribution in the flow channel along its length axis in case of (A) a basic, straight-channel junction point and (B) a narrowing of the flow channel at the junction point. For visualization of the diffusion, glucose at a concentration of 10 mM is introduced at a flow-rate of V1 = 100 μl/min. For the buffer flow, water was chosen at 40 μl/min. Each of the three images represents the concentration distribution of glucose at cross-sections for x = 2.2 mm (junction point), 5.0 mm and 30 mm (in front of biosensors).

a 10 mM glucose solution (in water, $D = 6.7 \times 10^{-10}$ m^2/s).[41] The three images in each column present the glucose concentration in cross-sections at x = 2.2 mm (junction point), 5.0 mm and 30 mm (just in front of the biosensors, *cf.* Fig. 1B). The change of the aspect ratio allows to generate a uniformly distributed buffer layer below the sample layer, whereas the basic channel shape results in the expected distribution of the buffer at the lower edges of the flow-through channel. Along the channel, glucose diffuses through the water layer resulting in a lower concentration at the bottom of the channel above the biosensor (at x > 30 mm). The position of the biosensors are indicated in the lowest images. For these calculations, the sample was introduced at a flow-rate of 100 μl/min, the buffer at 40 μl/min.

Optical inspections. The effect of the narrowing of the channel was also investigated using fluorescence and light microscopy. DI-water and a fluorescent solution (300 nM sodium fluorescein solution in DI-water) were pumped into the sample channel with a constant flow-rate of 100 μl/min respectively into the buffer channel at 20 to 60 μl/min. The intensity of the reflected light across the sample microchannel was measured at different flow-rates and analyzed using MATLAB. The profiles of these intensities are shown in Fig. 3A. The stable level of the intensity across the channel, and the respective shift of the level by increasing the flow-rate of the fluorescent liquid indicate the homogeneous spread of the top layer on the one beneath and compare well with the computed results. The linearity of the effect is shown in the insert of Fig. 3A. Fig. 3B shows three photographs with different flow-rates of the buffer solution and constant sample flow-rate. The introduction of clear DI-water beneath the blue-colored sample flow, leads to a homogenous color reduction across the channel dependent upon the flow-rate of the buffer solution. Both experimental observations thus reproduce well the computational results.

Biosensor characteristics

Fig. 4 shows a typical calibration measurement – here for glucose – of a microfluidic cartridge including a glucose and a lactate biosensor in parallel upon consecutive increase of the glucose concentration in the samples flow at 100 μl/min (third electrode not used here). The glucose biosensor shows the expected saturation for concentrations of more than 2 mM. No cross-talk is observed on the adjacent lactate biosensor even at high glucose concentrations (15 mM) emphasizing the advantage of laminar flow conditions and placement of the enzymatic membrane in a recess. This validates the approach for the multi-analyte detection.

Sensitivities of 157 ± 28 nA/mM (n = 6) for glucose sensors and 79 ± 12 nA/mM (n = 5) for lactate sensors were obtained at day 1 respectively day 3 after membrane deposition using the described protocol (see Experimental section). The low standard deviations emphasize the reproducible deposition of the enzymatic membranes on the microelectrodes using the on-chip focused dispensing. Even if the volume of the manually deposited droplet is not precisely controlled, the amount of immobilized enzyme, the lateral dimension and thickness of the enzymatic membrane is inherently defined by the design and fabrication of the channel.

The sensitivities of the biosensors were also characterized over time. Between measurements, the flow-through channel was filled with PBS and the cartridges were stored at 4 °C. A decrease of 7.4 nA mM^{-1} d^{-1} and 1.0 nA mM^{-1} d^{-1} was observed for the glucose and lactate biosensor over the first three weeks, respectively. At present, the glucose sensor shows a rather low lifetime and needs further optimization of the composition of the membrane. The higher stability of the lactate sensor might be a result of the higher BSA concentration in the formulation of the membrane solution stabilizing the enzyme. However, the problem of low storage lifetimes can be compensated by a functionalization just before use. This is strongly supported by the presented deposition method that can be performed after completed fabrication of the cartridge.

Adjustment of the linear response range

The calibration curve in Fig. 4 (insert) clearly shows the limitation of the biosensor regarding the linear response. Physiological relevant concentrations of glucose for example are up to 30 mM and require a sensor system with an adequate linear region. This is the reason why the biosensors are covered with a diffusion-limiting layer to reduce the concentration on top of the biosensor. The layer has to linearly scale the expected concentration range down to the linear response range of the biosensor. This factor FLR is primarily defined by the diffusion coefficient D and the diffusion length (= layer thickness).

The introduction of the buffer solution beneath the sample-flow acting as a dynamic diffusion-layer has the great advantage that the diffusion length can be controlled online and adapted to the specific application. This is achieved by controlling the

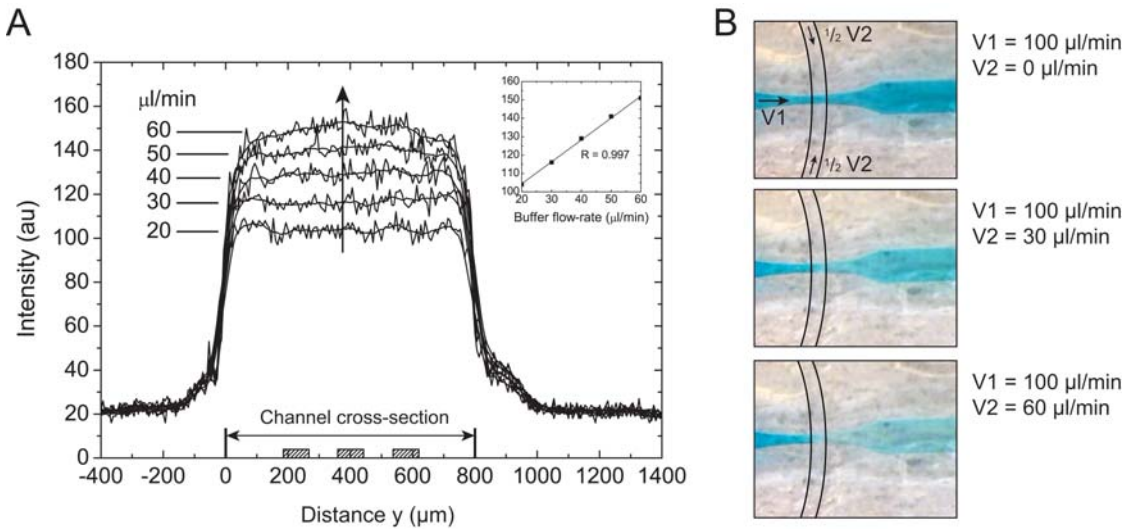

Fig. 3 (A) Fluorescent intensity (arbitrary unit, background-corrected) over the channel width at constant sample flow (transparent, 100 µl/min) and increasing buffer flow (fluorescent, 20–60 µl/min, 10 µl/min steps). Images were taken at x = 7.7 mm from the junction point and analyzed using MATLAB. Insert shows the linear relationship between the buffer flow-rate and the layer thickness (= fluorescence intensity). (B) Light microscopy images of colored sample flow (100 µl/min) and buffer flow without dye at different flow-rates.

flow-rate of the buffer solution. In literature, a dependency of the sensitivity and linear range with the sample flow-rate was reported[11] and used to adjust them. This effect is reasoned by the analyte that has to diffuse from the solution to the sensor surface in a limited amount of time. However, sample flow-rate is in most case dictated by the application. With our approach, the linear range can be adjusted with regards to the sample flow-rate. For equal linear ranges, high sample flow-rates require thinner diffusion layers than low sample flow-rates, because diffusion time is shorter. The diffusion time here is defined by the distance between the junction point and the biosensor at a specific sample flow-rate (= 28 mm).

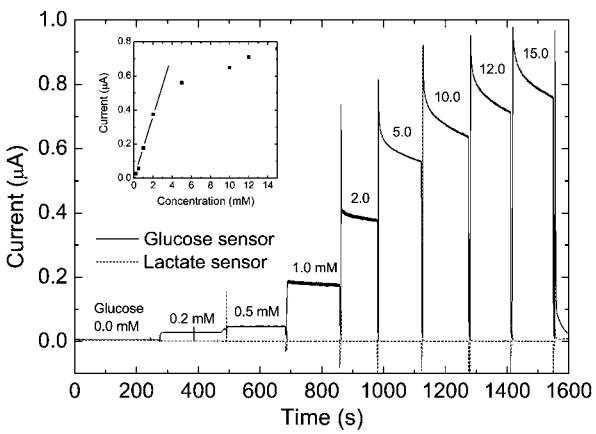

Fig. 4 Signal from GOx and LOx modified electrodes. Typical calibration measurement and curve (insert) upon consecutive pumping of samples with increasing glucose concentration through the sample channel (no buffer applied in this measurement). Only the glucose biosensor is responding by a proportional current increase. No signal is observed on the nearby lactate sensor.

Fig. 5 shows the result of a set of simulations varying sample and buffer flow-rate, concentration and position in the channel (see Fig. 1 and 2 for coordinates). First in 5A, the concentration profile is plotted in the middle (y = 400 µm) and along the length of the flow-through channel for x = 10 to 30 mm illustrating diffusion of glucose over length and time from the top (z = 0) to the bottom of the channel (z = 370 µm). 5B shows the concentration profiles at position x = 30 mm, but varying the y-position from 100 to 700 µm (*cf.* Fig. 2B, x = 30 mm). It illustrates the good lateral concentration uniformity, with only a minor variation near the channel walls for y = 100 and y = 700 µm, respectively. In both graphs, flow-rates were kept constant at V1 = 20 µl/min and V2 = 10 µl/min. Note that the chosen flow rates, especially V1, are lower, than in the flow rates indicated in Fig. 2 and 3 to increase diffusion times for better visibility.

In Fig. 5C, the concentration profiles at coordinates (x = 30 mm, y = 400 µm) are presented, again at constant flow-rates of V1 = 20 µl/min and V2 = 10 µl/min, but this time varying the inlet glucose concentration from 1 to 15 mM. The graph illustrates how the inlet concentration range of 0 – 15 mM is scaled down to 0–6.9 mM on the biosensor surface (x = 370 µm) in a linear way (see insert). The scaling factor FLR in this particular case is 0.46. It is a function of V1, V2 and the diffusion coefficient D. FLR can be determined for all combination of V1, V2 and target analytes with a defined D. Fig. 5D shows an example for glucose. The graph presents the relationship of FLR with the sample and buffer flow-rates. It can be used as a reference for the buffer flow-rate adjustment when sample-flow is given and an optimal sensitivity and linear range is required. The following virtual example shall illustrate its potential: A specific application requires a linear range up to 5 mM, the sample flow-rate is 50 µl/min. Assuming that the biosensor has a linear response up to 2 mM, a factor FLR of 0.4 is required. According to the calculated curve, V1/V2 has to be approximately

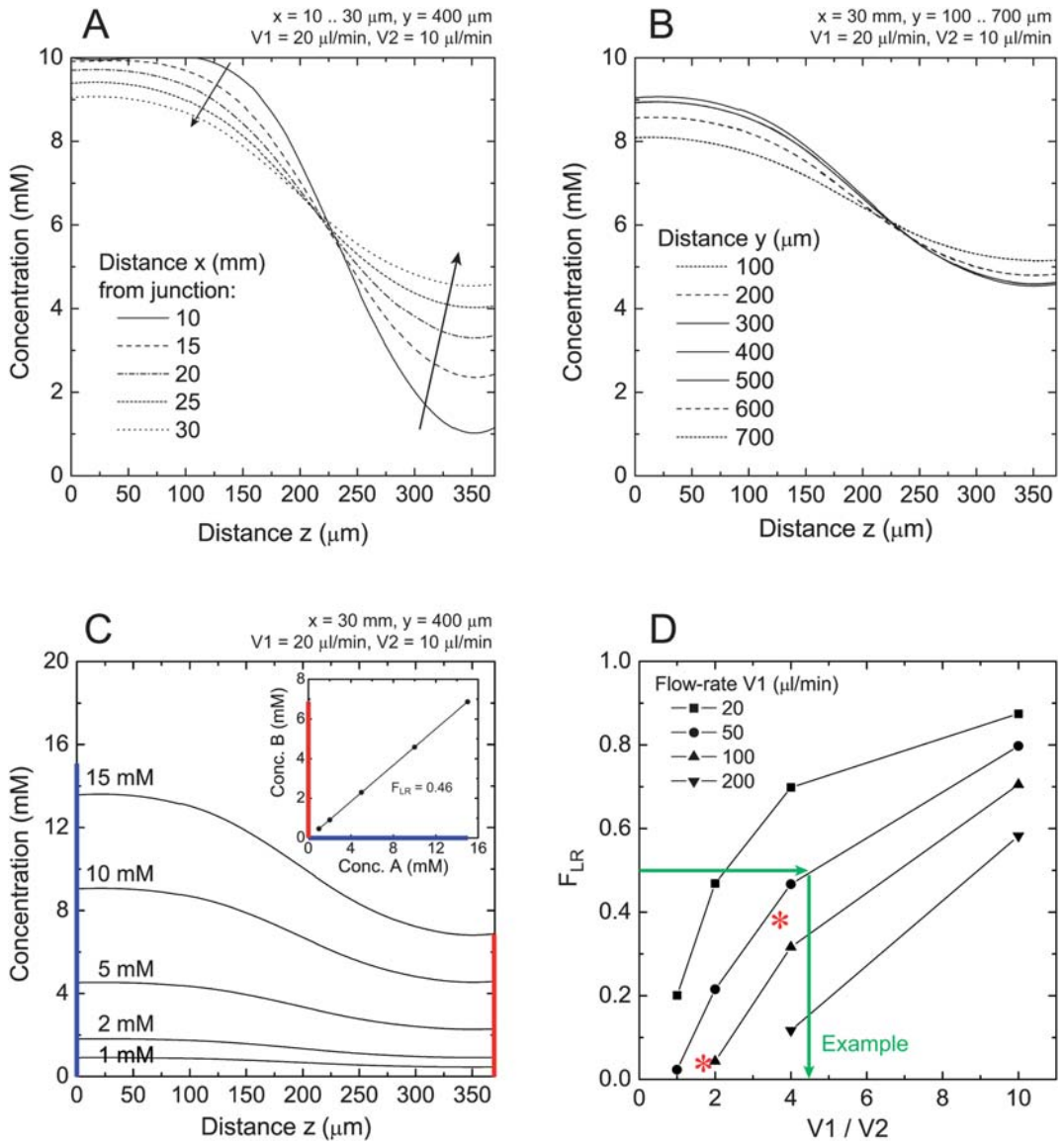

Fig. 5 Simulated concentration profiles for z = 0… 370 μm (top to bottom): (A) along the channel length at y = 400 μm with 10 mM glucose sample solution, (B) in front of the biosensors at x = 30 mm (biosensors start at x = 30.2 mm) and at different y-positions with 10 mM glucose sample solution, and (C) at (x, y) = (30 mm, 400 μm) and varying inlet glucose concentrations. Insert (C) shows the linear correlation between inlet concentration and concentration on the biosensor surface. (D) Correlates FLR with the flow-rate ratio V1/V2 (experimental data indicated by a red *).

4.5 resulting in V2 = 11.1 μl/min. With this buffer flow-rate the biosensor cartridge is operated at an optimal sensitivity and adequate linear response range.

Fig. 6 and Table 1 present typical calibration curves of a glucose (solid trace) and a lactate biosensor (dashed trace) where sensitivity and linear region are experimentally adjusted. The sample flow-rate is kept constant at 100 μl/min, whereas the buffer flow-rate is varied between 0 and 65 μl/min (buffer solution = PBS). For a stable and continuous sheath-flow good fluidic connections, precise control of the flow-rate and continuity in pumping is required. When changing the buffer flow-rate, the new diffusion layer thickness is set up rapidly and stabilizes within seconds. We observed a stable biosensor current response at constant sample concentration. Further, the diffusion layer has no effect on the noise level of the biosensor.

The curves in Fig. 6 nicely shows the adaption of the linear range when changing flow-rate V2. Calculating the corresponding, experimental factors FLR for the glucose sensor and placing them in graph D of Fig. 5 (red *), a good correlation with the simulated curves can be found. It emphasizes the flexibility and performance of this simple and inexpensive microfluidic cartridge.

Experimental section

Computational fluid dynamics (CFD)

FEM simulations have been carried out using the COMSOL Multiphysics simulation software (3D chemical engineering module using Laminar Flow with incompressible Navier–Stokes equations combined with Mass Transport considering diffusion

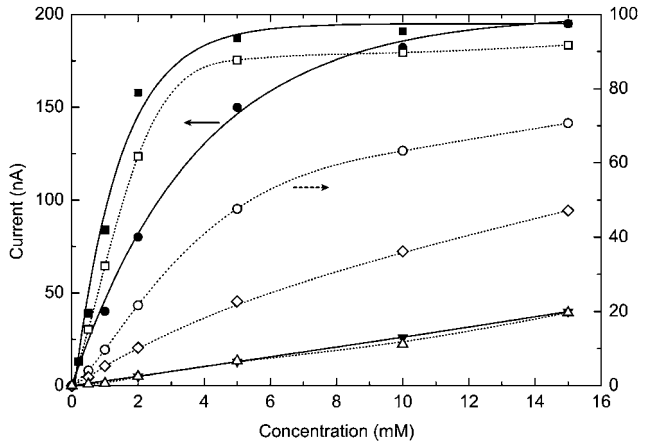

Fig. 6 Calibration curves for the glucose (solid trace) and the lactate biosensor (dashed trace) at a constant sample flow-rate of 100 µl/min and different buffer flow-rates: 0 µl/min (■/□), 30 µl/min (●/○), 45 µl/min (◇) and 65 µl/min (▼/△).

Table 1 Sensitivity and linear response range in dependency of the buffer flow-rate (sample flow-rate: 100 µl/min)

Buffer [µl/min]	Glucose		Lactate	
	S [nA/mM]	LR [mM]	S [nA/mM]	LR [mM]
0	84.0	1.5	32.2	2
30	40.0	2.0	9.7	4
45	—	—	3.6	8
65	2.6	15.0	1.1	15

and convection). The geometries of the junction point and flow-through channel were exactly reproduced. For simplicity, three-dimensional calculations were only performed for glucose using a diffusion coefficient of $D = 6.7 \times 10^{-10}$ m^2/s and water as liquid media.[41]

Chemicals

The following chemicals for clean-room related work were obtained from Microchem Corp., USA: lift-off resist LOR 3B, PG Remover, SU-8 50, and SU-8 100. Positive photoresist S1813 was purchased from Shipley, PGMEA from Sigma Aldrich, Switzerland. 4-inch Pyrex wafers with a thickness of 500 µm came from Schott, Switzerland.

Sylgard 184 (PDMS) was purchased from Dow Corning, USA. Bovine serum albumin (BSA), glutaraldehyde solution (GA, 25% in water), D-(+)-glucose anhydrous, sodium L-lactate and Triton-X 100 were acquired from Fluka, Switzerland. 0.01 mM phosphate buffer saline (PBS) was prepared by mixing 1.367 g of $Na_2HPO_4 \cdot 2H_2O$, 0.368 g of $NaH_2PO_4 \cdot H_2O$, 9 g of NaCl (all from Merck) in 1 l of DI-water and adjusted to pH 7.2. Fluorescein sodium salt, 3-aminopropyltriethoxysilane (APTES), chlorodimethyloctadecylsilane, glucose oxidase (GOx) and lactate oxidase (LOx) were obtained from Aldrich.

Fabrication

Operation and layout were optimized to simplify the fabrication and achieve a low-integrated microfluidic cartridge. The presented prototype consists of three layers – the Pyrex substrate with patterned metal electrodes, a structured SU-8 middle-layer and a replica-molded PDMS top-layer[42] (Fig. 7). The rapid prototyping technique allows fabricating the cartridge within a minimal amount of time.

Bottom layer. Patterning of the Pt-metal on a 4-inch Pyrex wafer is done according to the following procedure: The photoresists LOR 3B and S1813 are subsequently spin-coated on the substrate. After UV exposure and development, a 20 nm Ti adhesion layer and 130 nm Pt layer are deposited on the Pyrex substrate by evaporation. Development (lift-off) in PG Remover completes the metal structuring.

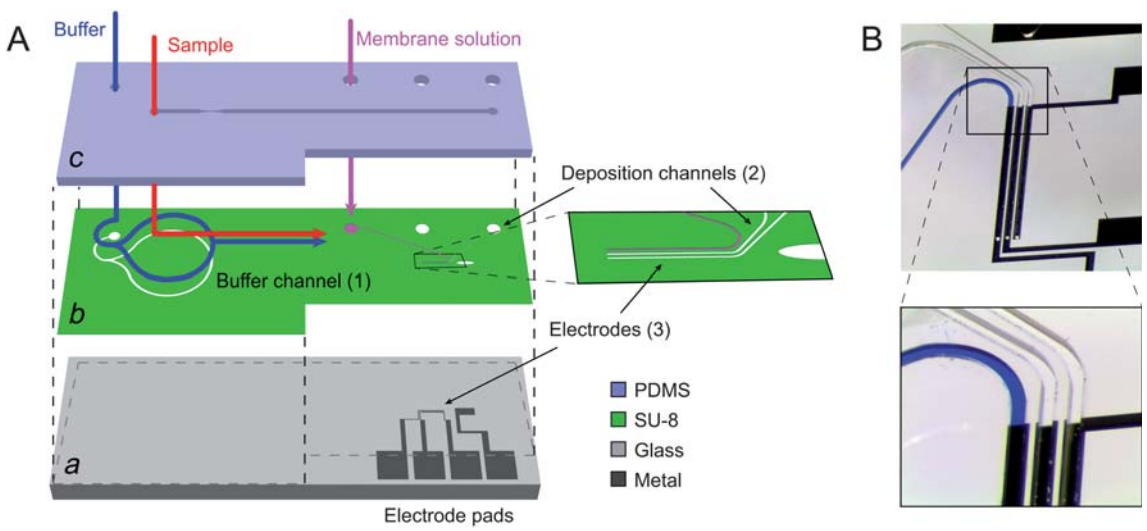

Fig. 7 (A) The microfluidic cartridge consists of three layers: a) the Pyrex substrate with a patterned Pt layer, b) an SU-8 layer comprising the buffer channel and the deposition channels, and c) a PDMS cover with the sample channel and fluidic access holes. All layers are irreversibly connected together. (B) Photograph and close-up view of the parallel-arranged electrodes – the left one is covered with a colored, enzymatic membrane.

SU-8 layer. The SU-8 layer comprises three functionalities (see Fig. 7): It contains (1) the buffer channel allowing to introduce the diffusion layer beneath the sample flow, (2) the deposition channels to functionalize the microelectrodes with enzymatic membranes and (3) in the same time, the end of the deposition channels form the microelectrodes. Note that the SU-8 is also the top passivation leaving the metal uncoated only over the electrode and bond-pad sites.

Procedure: After dehydration, an 80-μm-thick SU-8 50 layer is spin-coated on the Pyrex wafer and soft-baked on a hot plate (slow temperature ramps are used to reduce internal stress). The SU-8 layer is exposed to UV light through an aligned mask for structuring. After the post bake the unexposed SU-8 is developed by immersion of the wafer in PGMEA for 10 min.

Cover layer. The top layer contains the sample channel with in- and outlet and the access holes of the deposition area. It is fabricated out of PDMS by replica molding using an SU-8 master. SU-8 100 is spin-coated on a 4-inch silicon wafer with a thickness of 370 μm, this is followed by a soft bake (25 min at 65 °C, 80 min at 95 °C). The layer is patterned by UV exposure using a mask, following the soft post-exposure bake, it is developed in PGMEA to create the SU-8 master. Before molding, the master undergoes a vapor silanization to reduce PDMS adhesion: For this the wafer is placed in a vacuum chamber together with a droplet (1 - 2 μl) of chlorodimethyloctadecylsilane for two hours. The PDMS part is then fabricated as follows: Freshly mixed PDMS (10 : 1 w/w) is poured on the SU-8 master, degassed for one hour and cured in an oven for 2 h at 65 °C). The 2 mm-thick PDMS layer is gently peeled off and cut along the contour of the cartridge.

Bonding. The PDMS layer is irreversibly bonded to the SU-8 layer to seal the microfluidic channels and complete the fabrication of the cartridge. The bonding process is performed using a vapor silanization that was previously reported by our group.[43] Both the SU-8 and PDMS layers are cleaned thoroughly with isopropanol and DI-water. The SU-8 layer is then silanized with 3-aminopropyltriethoxysilane (APTES) in a closed chamber for two hours. Finally, the two surfaces are brought into contact and heated on a hotplate (10 min at 70 °C). The fabricated cartridge is shown in Fig. 8A.

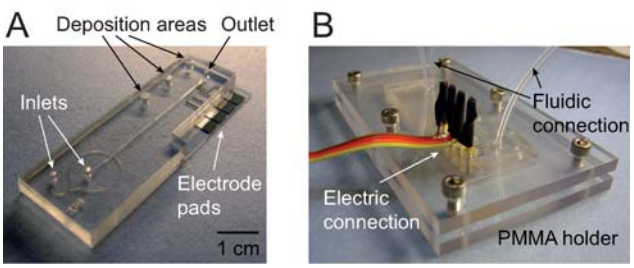

Fig. 8 (A) Fabricated cartridge comprising all fluidic access holes and connection pads. (B) PMMA holder ensuring reliable electrical and fluidic connections.

Functionalization

For the detection of glucose and L-lactate, two different functional layers containing GOx and LOx, respectively, are deposited on the microelectrodes. These membranes are formed by a co-cross-linking of the enzymes with the bi-functional agent glutaraldehyde (GA) and bovine serum albumin (BSA). The ingredients of the membranes were first mixed carefully in an aqueous solution: For the glucose biosensor 2 mg GOx, 3.5 mg BSA, 125 μl DI-water, 125 μl Triton-X 100 (3 g/l) and 20 μl glutaraldehyde (25%), while for the lactate biosensor 2.5 mg of LOx, 35 mg of BSA, 125 μl of DI-water, 125 μl of Triton-X 100 and 5 μl of glutaraldehyde were used. Once prepared, a small droplet is manually pipetted into the specifically designed deposition areas. A few minutes after deposition, the membranes are completely cross-linked on the microelectrodes. The nonionic surfactant Triton-X 100 is added to the deposition liquid to overcome the hydrophobicity of the microchannels structured in SU-8 and PDMS, and let capillary forces drag the membranes towards the microelectrodes.

Assembly and operation

For operation, the cartridge is placed in a PMMA holder. It is fabricated of two structured plates (bottom and lid), which sandwich the cartridge in the middle using small screws. Spring contacts embedded in the lid provide electrical contact to the electrode pads. Three holes in the lid allow the fluidic tubing being connected to the two inlets and the outlet of the cartridge (Fig. 8B). A constant potential of 0.7 V is applied between each working electrode and the common Pt pseudo-reference/counter electrode on the cartridge using a 4-channel multi-potentiostat (eDAQ, Australia). Continuous liquid-flow of sample and buffer solution is independently controlled by two calibrated syringe pumps (Harvard Apparatus, USA). Samples consisted of PBS prepared with defined glucose and lactate concentrations, the diffusion layer was PBS.

Conclusion

We developed a microfluidic device whose design was optimized for the use of rapid soft lithography techniques to fabricate a low-integrated prototype. It covers the needs of the concept of mass-fabricated, low-cost and disposable cartridges outsourcing electrical and fluidic control to a desktop unit. The cartridge enables simultaneous and continuous detection of several analytes without cross-talk, demonstrated by the integration of a glucose and lactate biosensor in a flow-through channel. The biosensors are created by functionalization of microelectrodes using on-chip focused dispensing. This allows a reproducible and spatially controlled immobilization of specific enzyme membranes on closely-placed microelectrodes after completed fabrication of the cartridge. Therefore cartridge fabrication and functionalization are divided into two independent steps. With minor adaptions, this method can be used to integrate further sensors based on the same principle (*e.g.* choline, glutamate) or to coat one of the electrodes with an inactive BSA membrane to remove interferences by the differential method. The linear response range and sensitivity of the biosensor can be dynamically adjusted in accordance to its application. This was realized

taking advantage of the laminar-flow conditions and the introduction of a liquid diffusion layer beneath the sample flow. We optimized the sheath-flow and showed the adjustment of the linear response range by varying the flow-rate of the buffer solution in experiments and simulations. Next steps will include assessment of the cartridge with real samples, modification of the microelectrodes with other enzymes at a further optimization of the functionalization procedure.

Acknowledgements

This work is supported by the European integrated project NeuroProbes (www.neuroprobes.org, EU IP IST-027017). The authors also gratefully thank the staff at the Microsystems Technology Division of CSEM SA, Switzerland.

References

1 G. S. Wilson and R. Gifford, *Biosens. Bioelectron.*, 2005, **20**, 2388–2403.
2 J. Wang, *Talanta*, 2008, **75**, 636–641.
3 Z. M. Rong, E. Leitao, J. Popplewell, B. Alp and P. Vadgama, *IEEE Sens. J.*, 2008, **8**, 113–120.
4 M. Mascini, *Sens. Actuators, B*, 1992, **6**, 79–82.
5 W. Schuhmann, H. Wohlschlager, J. Huber, H. L. Schmidt and H. Stadler, *Anal. Chim. Acta*, 1995, **315**, 113–122.
6 C. R. Soccol, B. Marin, M. Raimbaultand and J. M. Lebeault, *Appl. Microbiol.*, 1994, **41**, 286–290.
7 D. Moscone, M. Pasini and M. Mascini, *Talanta*, 1992, **39**, 1039–1044.
8 Y. Okawa, H. Kobayashi and T. Ohno, *Anal. Chim. Acta*, 1995, **315**, 137–143.
9 E. Dempsey, D. Diamond, M. R. Smyth, G. Urban, G. Jobst, I. Moser, E. M. J. Verpoorte, A. Manz, H. M. Widmer, K. Rabenstein and R. Freaney, *Anal. Chim. Acta*, 1997, **346**, 341–349.
10 J. Perdomo, H. Hinkers, C. Sundermeier, W. Seifert, O. M. Morell and M. Knoll, *Biosens. Bioelectron.*, 2000, **15**, 515–522.
11 F. Palmisano, R. Rizzi, D. Centonze and P. G. Zambonin, *Biosens. Bioelectron.*, 2000, **15**, 531–539.
12 I. Moser, G. Jobst and G. A. Urban, *Biosens. Bioelectron.*, 2002, **17**, 297–302.
13 H. Nakamura, K. Tohyama, M. Tanaka, S. Shinohara, Y. Tokunaga, F. Kurusu, S. Koide, M. Gotoh and I. Karube, *Biosens. Bioelectron.*, 2007, **23**, 621–626.
14 O. Geschke, H. Klank and P. Tellemann, *Microsystem engineering of lab-on-a-chip devices*, Wiley-VCH, Weinheim, 2003.
15 R. S. Marks, *Handbook of biosensors and biochips*, Wiley, Chichester, 2007.
16 M. Suzuki and H. Akaguma, *Sens. Actuators, B*, 2000, **64**, 136–141.
17 M. Quinto, M. Koudelka-Hep and F. Palmisano, *Analyst*, 2001, **126**, 1068–1072.
18 J. Perdomo, C. Sundermeier, H. Hinkers, O. M. Morell, W. Seifert and M. Knoll, *Biosens. Bioelectron.*, 1999, **14**, 27–32.
19 H. Frebel, G. C. Chemnitius, K. Cammann, R. Kakerow, M. Rospert and W. Mokwa, *Sens. Actuators, B*, 1997, **43**, 87–93.
20 R. Kurita, K. Hayashi, O. Niwa, K. Torimitsu, K. Yamamoto and T. Kato, *Anal. Sci.*, 2001, **17**, i437–i439.
21 C. Jimenez, J. Bartroli, N. F. de Rooij and M. Koudelka-Hep, *Sens. Actuators, B*, 1995, **27**, 421–424.
22 G. Jobst, I. Moser, M. Varahram, P. Svasek, E. Aschauer, Z. Trajanoski, P. Wach, P. Kotanko, F. Skrabal and G. Urban, *Anal. Chem.*, 1996, **68**, 3173–3179.
23 C. Malitesta, F. Palmisano, L. Torsi and P. G. Zambonin, *Anal. Chem.*, 1990, **62**, 2735–2740.
24 D. J. Strike, N. F. de Rooij and M. Koudelka-Hep, *Biosens. Bioelectron.*, 1995, **10**, 61–66.
25 M. Koudelka, S. Gernet and N. F. de Rooij, *Sens. Actuators*, 1989, **18**, 157–165.
26 M. Kyrolainen, S. M. Reddy and P. M. Vadgama, *Anal. Chim. Acta*, 1997, **353**, 281–289.
27 E. Kim, Y. Xia and G. M. Whitesides, *Nature*, 1995, **376**, 581–584.
28 E. Delamarche, A. Bernard, H. Schmid, B. Michel and H. Biebuyck, *Science*, 1997, **276**, 779–781.
29 J. P. Brody, P. Yager, R. E. Goldstein and R. H. Austin, *Biophys. J.*, 1996, **71**, 3430–3441.
30 J. B. Knight, A. Vishwanath, J. P. Brody and R. H. Austin, *Phys. Rev. Lett.*, 1998, **80**, 3863–3866.
31 L. Pollack, M. W. Tate, N. C. Darnton, J. B. Knight, S. M. Gruner, W. A. Eaton and R. H. Austin, *Proc. Natl. Acad. Sci. U. S. A.*, 1999, **96**, 10115–10117.
32 H. Y. Park, X. Y. Qiu, E. Rhoades, J. Korlach, L. W. Kwok, W. R. Zipfel, W. W. Webb and L. Pollack, *Anal. Chem.*, 2006, **78**, 4465–4473.
33 C. Simonnet and A. Groisman, *Appl. Phys. Lett.*, 2005, **87**, 114104.
34 C. Simonnet and A. Groisman, *Anal. Chem.*, 2006, **78**, 5653–5663.
35 Y. Gambin, C. Simonnet, V. van de Linder, A. Deniz and A. Groisman, *Lab Chip*, 2010, **10**, 598–609.
36 G. S. Zhuang, T. G. Jensen and J. P. Kutter, *12th Int. Conference on Miniaturized Systems for Chemistry and Life Science (microTAS)*, San Diego, 2008, 1357–1359.
37 E. Kauffmann, N. C. Darnton, R. H. Austin, C. Batt and K. Gerwert, *Proc. Natl. Acad. Sci. U. S. A.*, 2001, **98**, 6646–6649.
38 O. Hofmann, P. Niedermann and A. Manz, *Lab Chip*, 2001, **1**, 108–114.
39 O. Hofmann, G. Voirin, P. Niedermann and A. Manz, *Anal. Chem.*, 2002, **74**, 5243–5250.
40 O. Frey, P. D. van der Wal, N. F. de Rooij and M. Koudelka-Hep, *Procedia Chem.*, 2009, **1**, 281–284.
41 D. R. Lide, *CRC handbook of chemistry and physics*, CRC Press, Boca Raton, 76th edn, 1995.
42 D. C. Duffy, J. C. McDonald, O. J. A. Schueller and G. M. Whitesides, *Anal. Chem.*, 1998, **70**, 4974–4984.
43 S. Talaei, O. Frey, P. D. van der Wal, N. F. de Rooij and M. Koudelka-Hep, *Procedia Chem.*, 2009, **1**, 381–384.

